

## PERFORMANCE-BASED SEISMIC ANALYSIS OF HIGHWAY E75 OVERPASS AT KOVILJ SEIZMIČKA ANALIZA STANJA NADVOŽNJAKA AUTOPUTA E75 KOD KOVILJA

Originalni naučni rad / Original scientific paper  
UDK /UDC: 625.745.12:624.042.7  
Rad primljen / Paper received: 07.03.2014.

Adresa autora / Author's address:

- <sup>1</sup>) University of Belgrade, Faculty of Civil Engineering  
<sup>2</sup>) University of Belgrade, Innovation Centre of the Faculty of Mech. Engineering, email: [simon.sedmak@yahoo.com](mailto:simon.sedmak@yahoo.com)  
<sup>3</sup>) University of Novi Sad, Faculty of Technical Sciences

### Keywords

- overpass
- earthquake
- non-linear pushover analysis (NPA)
- plastic hinges
- performance states

### Abstract

*Presented in this paper are the results of the analysis of seismic performances of an overpass founded on piles, in interaction with the soil, located over the E75 Highway Novi Sad - Belgrade, as part of the Kovilj loop. Applied methods include: non-linear static push-over (NSPA) analysis, target displacement analysis, parametric target displacement analysis, vulnerability and reliability analysis. The overpass is modelled and taken into consideration for seismic effects along its transverse direction as a 2D planar model. Modelling of elastic-plastic strain is performed using plastic hinges, whereas the development of non-linear strain is considered using the incremental-iterative method. It is determined that the failure mechanism of the system occurred because of the plasticization of column ends, and it is maintained as such until the end of the non-linear analysis, along with the changes of performance states in plastic hinges. System vulnerability analysis has shown that up until the point where  $S_a = 0.2g$ , nearly all levels of damage are initiated, however, already at values of  $S_a \approx 0.3g$ , significant damages to the overpass are expected along the transverse direction with the probability of  $P \approx 1$ . On the other hand, reliability analysis of the overpass shows that reliability of  $R > 0$  is achieved for  $S_a < 0.23g$  for levels of significant damage and for lower ones.*

### INTRODUCTION

Designing bridges in everyday engineering practice is based on the application of national or international technical regulations. More often than not, existing regulations do not define specific problems that may occur during designing of bridges with enough detail. Existing regulations, in most cases, are not in compliance with modern regulative, such as EN /7/, AASHTO /1, 2/ or CALTRANS /5/. On the other hand, even the application of modern regulations has certain limitations in analysing structural systems on a higher level, for example in modern earthquake engineering which requires employing of experts and specialists for these very sensitive issues. Experienced designers can solve bridge building problems in accordance to current regula-

### Ključne reči

- nadvožnjak
- zemljotres
- nelinearna „pushover“ analiza (NPA)
- plastični zglobovi
- stanja konstrukcije

### Izvod

*U ovom radu su predstavljeni rezultati analize seizmičke karakteristike nadvožnjaka, postavljenog na stubovima, u interakciji sa tlom, na lokaciji iznad autoputa E75 Novi Sad – Beograd, kao deo petlje Kovilj. Primenjene metode obuhvataju: nelinearna statička „pushover“ analiza (NSPA), analiza pomeranja tačke, parametarska analiza pomeranja tačke, analize osetljivosti na oštećenja i pouzdanosti. Nadvožnjak je modeliran i razmotren prema seizmičkim uticajima duž poprečnog pravca kao ravanski 2D model. Modeliranje elastoplastičnih deformacija je izvedeno plastičnim zglobovima, gde je razvoj nelinearnih deformacija sagledan primenom inkrementalne-iterativne metode. Utvrđeno je da mehanizam loma sistema izaziva pojava plastičnosti u završecima stuba, koja se održava sve do završetka nelinearne analize, zajedno sa promenama stanja konstrukcije u plastičnim zglobovima. Analiza osetljivosti sistema pokazuje da sve do momenta kada je  $S_a = 0.2g$ , oštećenja se iniciraju na skoro svim nivoima, međutim, već pri  $S_a \approx 0.3g$ , očekuju se značajna oštećenja nadvožnjaka u poprečnom pravcu, sa verovatnoćom  $P \approx 1$ . S druge strane, analiza pouzdanosti nadvožnjaka pokazuje pouzdanost  $R > 0$  za  $S_a < 0.23g$  za nivoe značajnih i manjih oštećenja.*

tions, but in many cases are unable to answer important questions, such as: level of global ductility of the bridge along specific directions; expected levels of non-linear strain in the bridge for a given level of seismic hazard; how much damage can be expected for various levels of seismic hazards; where and how can a local or global structural failure be expected?

Answers to the above questions, along with the application of modern regulations for design of structures can be provided by an integral approach of using computer mechanics, finite element method (FEM), structural dynamics, reinforced concrete (RC) theory of structures, non-linear analysis, plasticity theory, fracture mechanics, soil-structure interactions and statistics and probability. Interaction and integration of most of the disciplines mentioned above are

unified within the methodology for Performance-Based Earthquake Engineering (PBEE).

Within PBEE methodology, consideration of non-linear behaviour of bridges is based on, among other things, the application of non-linear static push-over analysis (NSPA). The basis of bridge calculations using non-linear seismic analysis and the formulating of Finite Element Method (FEM) are given in /12/. Shown and analyzed in /9/ are some aspects of design methodology during the conceptual stage and the selection of models for the analysis of concrete bridges commonly used for seismic effects. Additionally, comparative analysis of certain regulations for design of seismic-resistant bridge structures are also presented. Application of non-linear static push-over analysis in solving of problems related to bridges founded on piles is shown in /6, 15, 16, 22/, whereas a general approach to bridge analysis using NSPA is shown in /4, 14, 19/.

In this paper, results of classic design method and of the Performance-Based Seismic Design method are compared for a given structure - an overpass. For this purpose, non-linear static push-over analysis is applied for frame system along the transverse direction. The overpass is designed according to Serbian regulations and built at the section of E75 Highway Novi Sad-Belgrade, the Kovilj loop.

#### METHODOLOGY OF FAILURE ANALYSIS

The overpass is designed according to Serbian regulations /20/ which are older than modern regulations for design and analysis of bridge structures. Numerical modelling and analysis of static and dynamic effects are performed using SOFiSTiK software, whereas the approximation is performed using surface and line finite elements to form a 3D model of the structure /11/. Longitudinal overpass supports which are prefabricated and monolithized, are

modelled as surface supports. Along the transverse direction, the structural system of the overpass is modelled as a frame static system which includes the piles as well, and the soil interaction is introduced by using elastic springs. For these springs, the equivalent stiffness is defined for both pressure and tension. The constitutive model of material behaviour is linear-elastic, and linear elastic analysis is used for determining cross-section forces. For determining of seismic effects, the equivalent static method is used, whereas sizing is performed using stress-strain work diagrams according to PBAB 87, /18/. In case of concrete, this diagram is a parabolic-straight line, whereas in case of reinforced steel - a bilinear work diagram without kinematic hardening is used.

#### NUMERICAL MODELLING OF A NON-LINEAR SOIL-PILE INTERACTION

Numerical model of the overpass used for non-linear analysis is taken into consideration by applying the decomposition of overpass structure into sub-groups which are then considered in detail from the point of possibility of optimal modelling as a plane model. From the aspect of seismic effects and system strain, it is of particular interest to analyse the overpass structure along the transverse direction, hence only this direction is analyzed in this research. Figure 1 shows the 3D model of the overpass created as a solid using an especially emphasized transverse frame of the overpass.

The overpass consists of two spans of 24 m each, whereas the transverse cross-section is made of 9 hollowed-out prefabricated elements with dimensions of 95/100 cm, with a span of 16.3 m. Central columns are of a circular cross-section with  $\varnothing 90$  cm and length of 5.9 m, connected to piles with  $\varnothing 130$  cm and length of 14.2 m via RC cubes

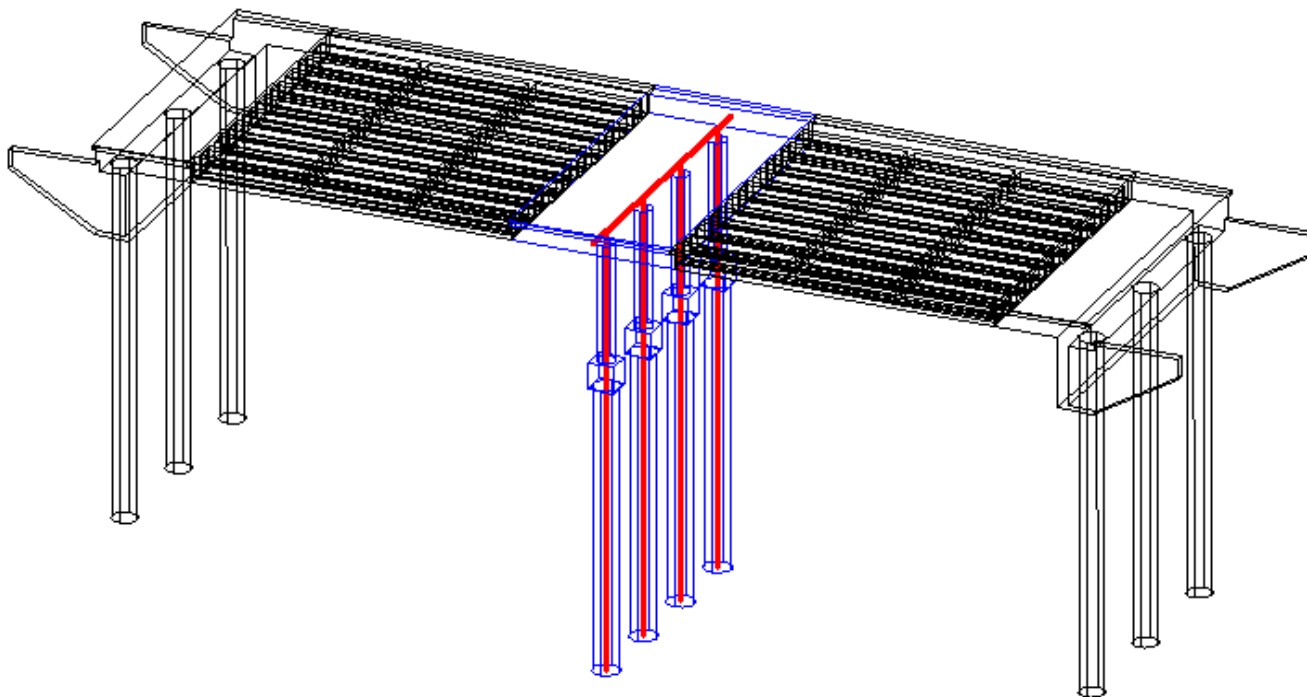


Figure 1. 3D model of the overpass created as a solid model with emphasized transverse frame.

Slika 1. 3D model nadvožnjaka sačinjen kao čvrsti model sa izvođenjem poprečnog rama.

with side length of 130 cm. Total width of the overpass is 16.33 m, whereas the plate in the central part has a height of 115 cm and width of 800 cm. Effective beam width is determined according to /13/ in such a way that it corresponds to the width of the plate in the central part of the overpass. The beam is made of MB 40 concrete, while MB 30 is used for columns and piles. Columns, piles and beams are modelled using linear finite elements, while the discretization is performed using the principle that the maximum element size is 0.5 m and the minimal number of elements per beam is 5. By applying these linear finite elements, the effect of transverse forces on total strain is also taken into account. Plasticization of the system takes place at locations of local plasticization - plastic hinges, therefore, 74 plastic hinges are applied. For the beam, plastic hinges are defined at places where plasticization is enabled via bending moments, whereas in case of columns, plastic hinges are defined at locations where plasticization occurred through the interaction of normal forces and bending moments. Stirrups, for both beams and columns, are assumed to remain closed during the development of plastic strain in the system. Plastic hinges of the beam and columns are applied at ends, while in case of piles, they are applied uniformly along the length. Column-beam ties are realised by using rigid elements (end length offset) with stiffness factor  $R = 1$ .

Soil-pile interaction is covered by applying link elements, hence a sophisticated hysteresis interaction model with incorporated contact elements (gap element) for simulation of reactions to pressure is applied. Backbone curves of a hysteresis model are defined as multi-linear  $p$ - $y$  curves according to /17/, in such a way that the tangent stiffness is determined from discrete values of force and displacements that changes along soil depth. In addition, when these curves are generated, the effects of groundwater level, defined according to the geotechnical profile of soil, are taken into account. Figure 2a shows the model of a transverse frame with defined elements for soil-pile interaction and Fig. 2b shows the same model with applied plastic hinges.

#### NSPA ANALYSIS OF AN OVERPASS IN THE TRANSVERSE DIRECTION

Non-linear static pushover analysis (NSPA) is performed for a non-linear model of structural behaviour, whereas seismic effects are generated and applied to the structure in form of seismic forces. Total response of the structure is non-linear and is considered within the capacity domain by applying an incremental-iterative method (Newton-Raphson method). General consideration of NSPA consists of two parts. First part includes the calculation on a real system with multiple degrees of freedom (MDOF). Generation of seismic forces is developed in several variants, ranging from the conventional approach and modal analysis to adaptive approach. In this paper, three procedures for generating of seismic forces are applied: as seismic load; based on inertial seismic forces (accel) and according to the first mode. Anyhow, recommendations according to regulations suggest the use of three or more procedures for generating of seismic forces in NSPA.

Each analysis is performed using SAP 2000 software, /21/. Material non-linearity is introduced via development of elastic-plastic strain in plastic hinges, whereas the geometry non-linearity includes  $P$ - $\Delta$  effects and large displacements. Non-linear static analysis of effects of vertical load is performed first, where the stiffness matrix of the system obtained at the end of this analysis is used as the initial matrix for NSPA. Load from the non-linear static analysis of effects of vertical loads is transferred and used in NSPA, so that the overpass analysis in realistic seismic conditions can be simulated. The first analysis is performed by controlling the load increment, whereas the second (NSPA) is performed by controlling the displacement increment. Maximum available structural displacement is determined using an iterative procedure, by gradually increasing displacement and controlling the number of increments realized. Figure 3 shows generated NSPA pushover curves for the applied: seismic forces (load); inertial forces (accel) and according to the first mode, as a function of global drift and relative value of the total shear force. For all applied methods of generating seismic forces, almost identical

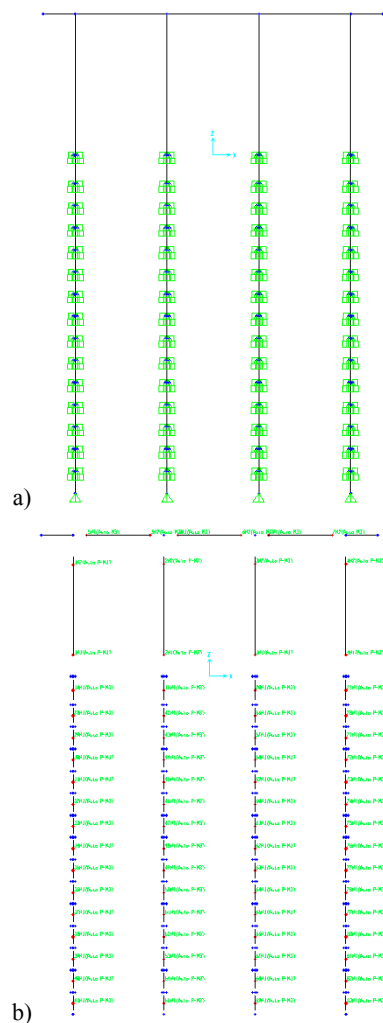


Figure 2. Transverse frame model with: a) defined elements for soil-pile interaction, b) applied plastic hinges.

Slika 2. Model poprečnog rama sa: a) definisanim elementima interakcije tlo-stub, b) primenom plastičnog zgloba

values of global drifts are realized. The shapes of all NSPA pushover curves are nearly identical, the only difference appearing in relative values of total shear force. Highest relative values of the total shear force are obtained for seismic force generation using inertial forces. This is caused by the influence of both the first mode and higher modes of a total system response, especially the third, fourth and eleventh.

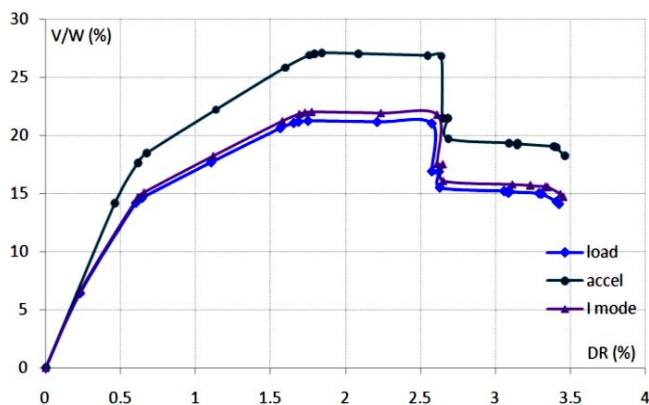


Figure 3. Generated NSPA pushover curves for applied seismic forces (load), inertial forces (accel) and according to first mode (I)  
Slika 3. Generisane NSPA *pushover* krive za zadate seizmičke sile (opterećenja), inercijalne sile (*accel*) u prvom modu (I)

Monitoring of plasticization systems (development of plastic hinges along incremental stages) via performance states: A, B, IO, LS, CP, C, D and E for applied seismic forces, inertial forces, according to first mode, are shown in Fig. 4. Values of global drifts and achieved performance states are given on the abscissa, whereas the number of plastic hinges  $N_{pl}$  that is achieved in specific inter-performance states A-B, C-IO, IO-LS, LS-CP, CP-C, D-E and >E are given on the ordinate. Performance state IO is a state of *immediate occupancy*, LS is the state of *life safety* and CP is *collapse prevention* of structures. Performance states A, B, C, D and E are the nodes on the backbone curve used for defining of a normalized force (moment) of plasticization in a single hinge. The number of plastic hinges has been nullified and is not shown in the figure for performance state A-B, since it is actually an elastic state. The number of plastic hinges and distribution of achieved performance states in case of applied seismic forces and according to the first mode is nearly identical, whereas in case of seismic forces generated as inertial, they are somewhat different. This difference is reflected in the number of formed plastic hinges for specific values of global drifts.

The second part of NSPA includes determination of the level of target displacement (target displacement analysis) of the overpass, hence following methods are used for the purpose of this research: Capacity spectrum method (CSM), according to ATC 40 /3/ and Equivalent Linearization Method (ELM), according to FEMA 440, /8/. CSM is performed in acceleration-displacement response spectra (ADRS) format, whereas ELM is performed in modified acceleration-displacement response spectra (MADRS) format.

Level of target displacement is determined according to iteration, and graphic presentation of target displacement

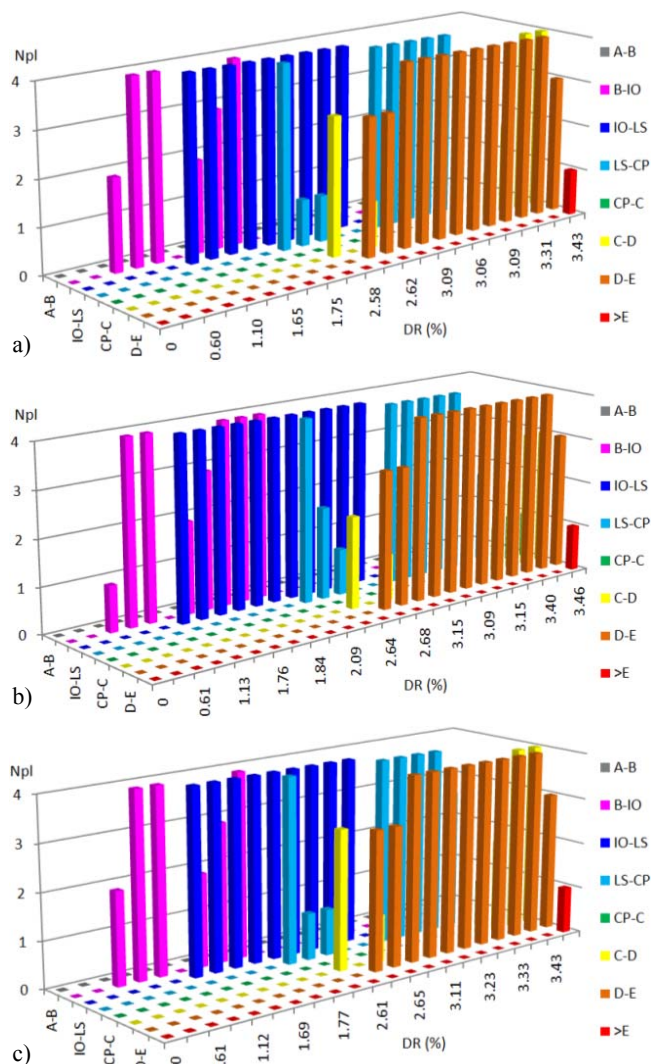


Figure 4. Monitoring of system plasticization (development of plastic hinges along incremental stages) via performance states: A, B, IO, LS, CP, C, D and E for applied: a) seismic forces (load), b) inertial forces (accel), c) according to the I-mode.

Slika 4. Praćenje plastičnosti sistema (razvoj plastičnih zglobova duž inkrementalnih stanja) preko stanja konstrukcije: A, B, IO, LS, CP, C, D i E za: a) seizmičke sile (opterećenje), b) inercijalne sile (*accel*), c) prema I modu

levels is represented using *capacity curves* and *demand curves*. Previously, discrete values of pushover curves are converted into capacity curves. Figures 5-7 show the created spectral curves, radial curves of vibration period  $T$ , capacity curves and seismic demand curves for the applied: seismic forces, inertial forces and first mode, for CSM method and ELM methods, respectively. Spectral curves in these figures are shown as sets of curves with various values of dampening coefficient in the interval of  $\xi = 5\%$  to  $20\%$ , and vibration periods are shown as sets of radial curves in the interval of  $T = 0.5$  to  $2$  s. Values of target displacements  $D_t$  along with the corresponding total shear forces  $V_t$  determined by using the CSM method are slightly less than the ones determined by ELM method. Corresponding values of spectral displacements  $S_d$  and spectral accelerations  $S_a$  are also slightly lower.

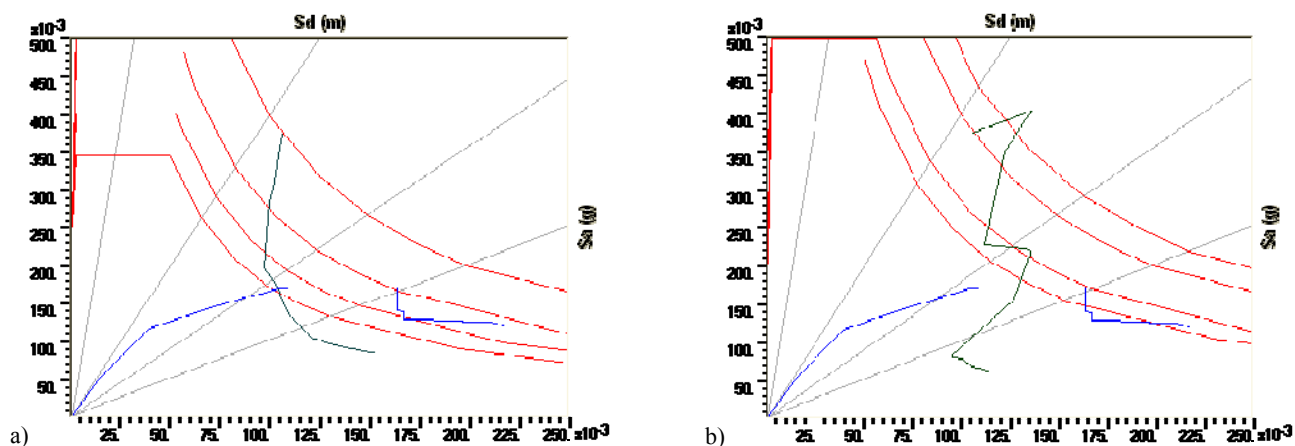


Figure 5. Created spectral curves, radial curves of the vibration period, capacity curves and seismic demand curves for applied seismic forces as pushover load: a) CSM method, b) ELM method.

Slika 5. Spektralne krive, radijalne krive perioda vibracija, krive nosivosti i seizmičke krive za primenjene seizmičke sile kao *pushover* opterećenje: a) CSM metoda, b) ELM metoda

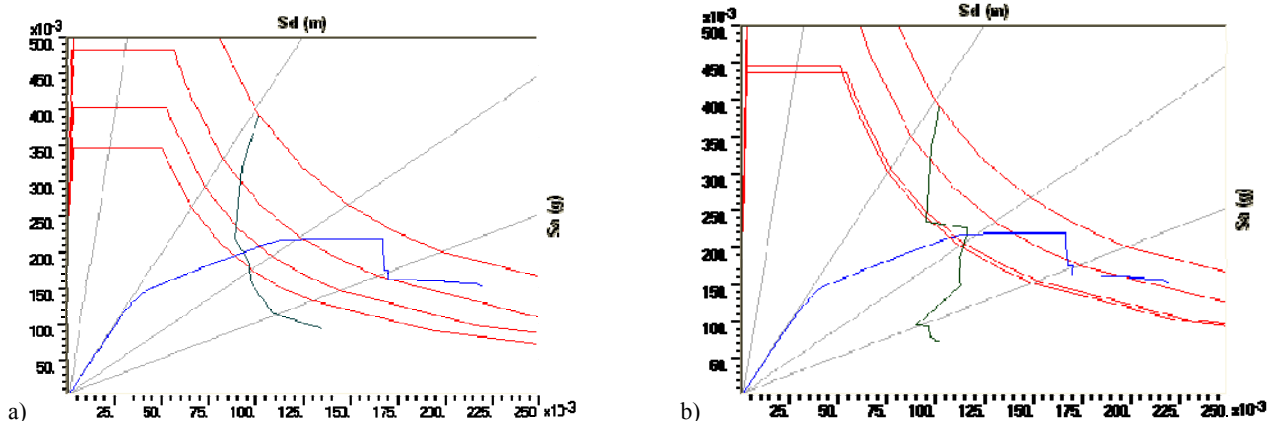


Figure 6. Spectral curves, radial curves for vibration periods, capacity curves and seismic demand curves for inertial forces as pushover load: a) CSM method, b) ELM method.

Slika 6. Spektralne krive, radijalne krive perioda vibracija, krive nosivosti i seizmičke krive za primenjene seizmičke sile kao *pushover* opterećenje: a) CSM metoda, b) ELM metoda

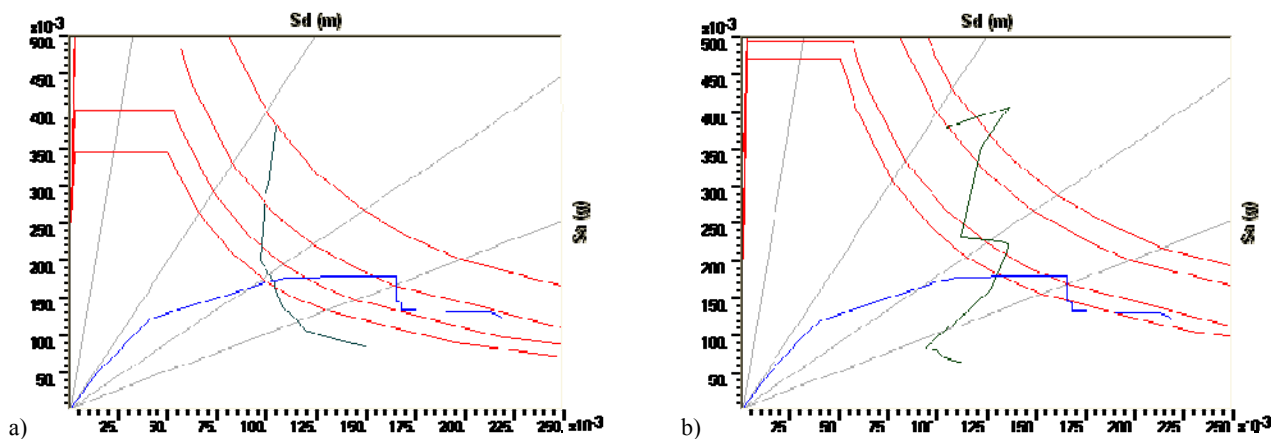


Figure 7. Spectral curves, radial curves for vibration periods, capacity curves and seismic demand curves according to first mode as pushover load: a) CSM method, b) ELM method.

Slika 7. Spektralne krive, radijalne krive perioda vibracija, krive nosivosti i seizmičke krive prema prvom modu kao *pushover* opterećenje: a) CSM metoda, b) ELM metoda

Parameter analysis of target displacement is performed for the applied seismic forces and for inertial seismic forces as pushover load, since modelling of seismic forces according to the first mode resulted in solutions extremely similar

to those obtained by directly applied seismic forces. Parameters  $C_a$  and  $C_v$  are considered in the interval of 0.1 to 1, and levels of target displacements are determined for these values using CSM and ELM methods. A total of 400 target

displacement analyses are carried out for target displacement levels calculated in this way by using parameter analysis. The following is taken into consideration and shown: displacement  $D_t$  (Fig. 8), total shear force  $V_t$  (Fig. 9), spectral displacement  $S_{d,t}$  (Fig. 10), spectral acceleration  $S_{a,t}$  (Fig. 11), vibration period  $T_t$  (Fig. 12), damping  $\xi_t$  (Fig. 13) and ductility  $\mu_t$  (Fig. 14) for applied seismic forces as pushover load. In cases where it was not possible to obtain a solution (level of target displacement could not be determined), because of impossibility of achieving intersection

between the capacity and demand curve, values  $D_t$ ,  $V_t$ ,  $S_{d,t}$ ,  $S_{a,t}$ ,  $T_t$ ,  $\xi_t$  and  $\mu_t$  are equal to zero.

For levels of target displacements calculated using parameter analysis, using inertial seismic forces as pushover load, the following is considered and shown: displacement  $D_t$  (Fig. 15), total shear force  $V_t$  (Fig. 16), spectral displacement  $S_{d,t}$  (Fig. 17), spectral acceleration  $S_{a,t}$  (Fig. 18), vibration period  $T_t$  (Fig. 19), damping  $\xi_t$  (Fig. 20) and ductility  $\mu_t$  (Fig. 21).

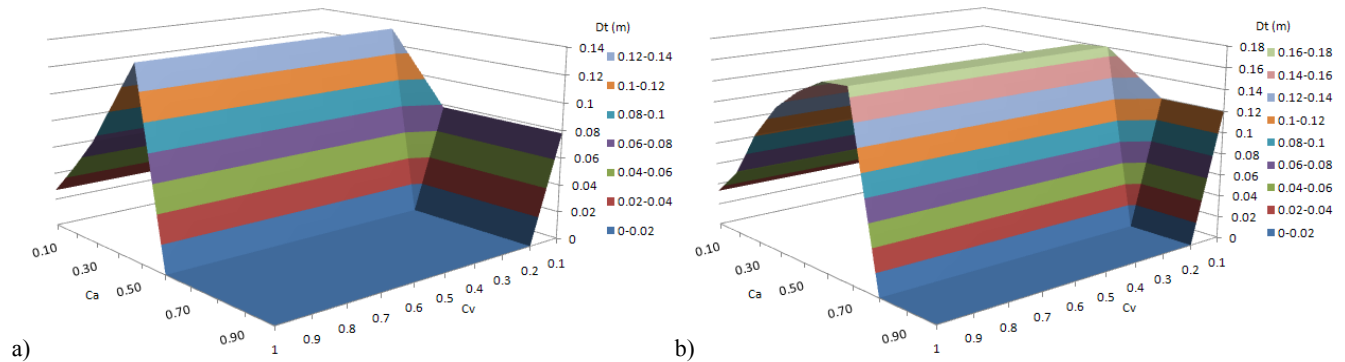


Figure 8. Values of displacement  $D_t$  obtained from  $C_a$  and  $C_v$  parameter analysis of target displacement for applied seismic forces as pushover load: a) CSM method, b) ELM method.

Slika 8. Vrednosti pomeranja  $D_t$  dobijenih preko  $C_a$  i  $C_v$  parametarske analize pomeranja tačke za primenjene seizmičke sile kao *pushover* opterećenje: a) CSM metoda, b) ELM metoda

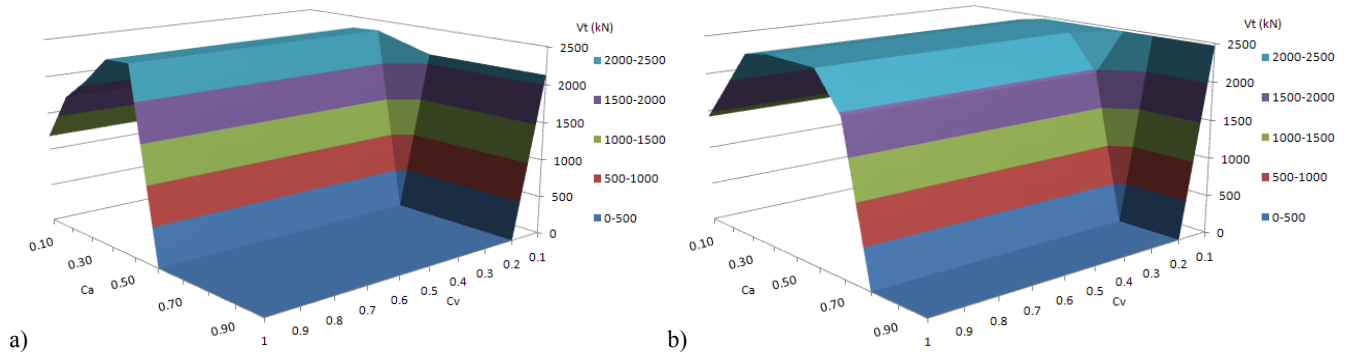


Figure 9. Values of shear force  $V_t$  obtained from  $C_a$  and  $C_v$  parameter analysis of target displacement for applied seismic forces as pushover load: a) CSM method, b) ELM method.

Slika 9. Vrednosti sila smicanja  $V_t$  dobijenih preko  $C_a$  i  $C_v$  parametarske analize pomeranja tačke za primenjene seizmičke sile kao *pushover* opterećenje: a) CSM metoda, b) ELM metoda

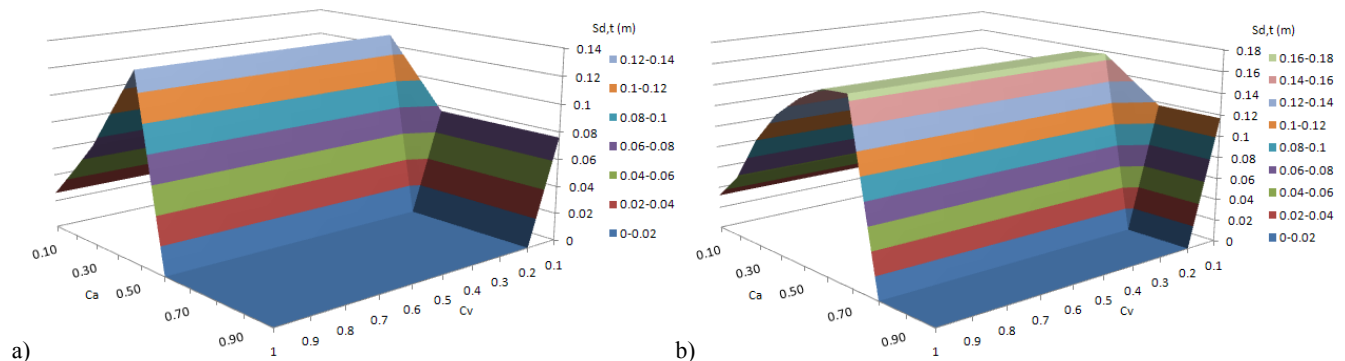


Figure 10. Values of spectral displacement  $S_{d,t}$  obtained from  $C_a$  and  $C_v$  parameter analysis of target displacement for applied seismic forces as pushover load: a) CSM method, b) ELM method.

Slika 10. Vrednosti spektra pomeranja  $S_{d,t}$  dobijenih preko  $C_a$  i  $C_v$  parametarske analize pomeranja tačke za primenjene seizmičke sile kao *pushover* opterećenje: a) CSM metoda, b) ELM metoda

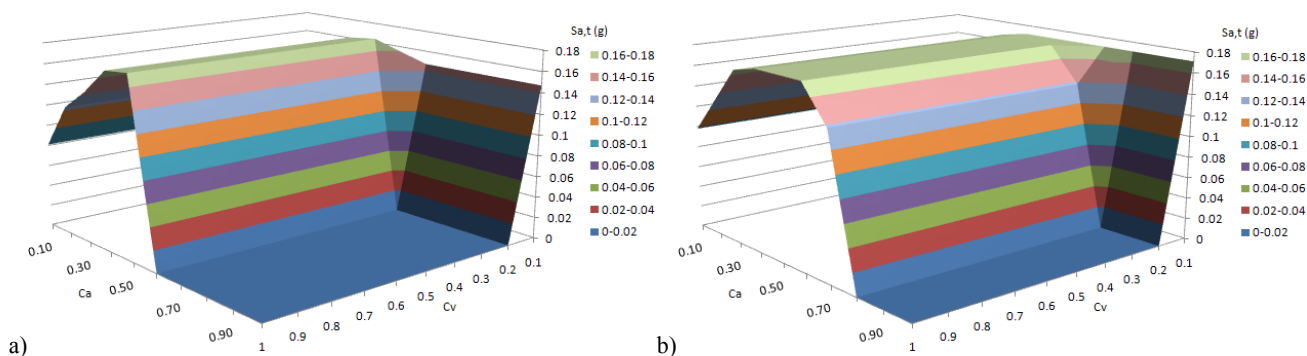


Figure 11. Values of spectral acceleration  $S_{a,t}$  obtained from  $C_a$  and  $C_v$  parameter analysis of target displacement for applied seismic forces as pushover load: a) CSM method, b) ELM method.

Slika 11. Vrednosti spektra ubrzanja  $S_{a,t}$  dobijenih preko  $C_a$  i  $C_v$  parametarske analize pomeranja tačke za primenjene seizmičke sile kao *pushover* opterećenje: a) CSM metoda, b) ELM metoda

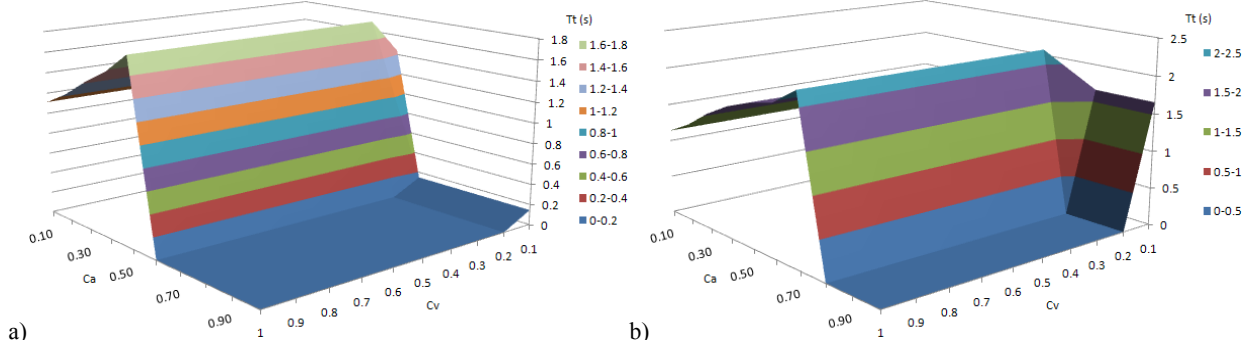


Figure 12. Values of vibration period  $T_t$  obtained from  $C_a$  and  $C_v$  parameter analysis of target displacement for applied seismic forces as pushover load: a) CSM method, b) ELM method.

Slika 12. Vrednosti perioda vibracija  $T_t$  dobijenih preko  $C_a$  i  $C_v$  parametarske analize pomeranja tačke za primenjene seizmičke sile kao *pushover* opterećenje: a) CSM metoda, b) ELM metoda

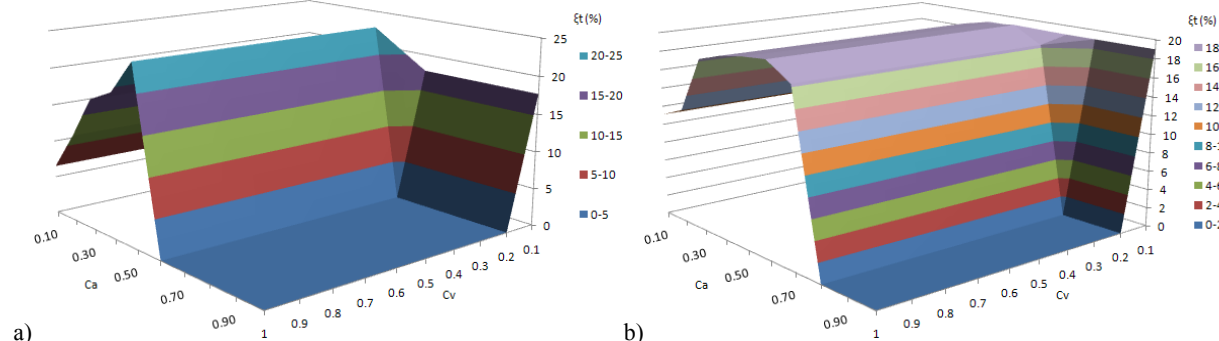


Figure 13. Values of dampening  $\xi_t$  obtained from  $C_a$  and  $C_v$  parameter analysis of target displacement for applied seismic forces as pushover load: a) CSM method, b) ELM method.

Slika 13. Vrednosti prigušenja  $\xi_t$  dobijenih preko  $C_a$  i  $C_v$  parametarske analize pomeranja tačke za primenjene seizmičke sile kao *pushover* opterećenje: a) CSM metoda, b) ELM metoda

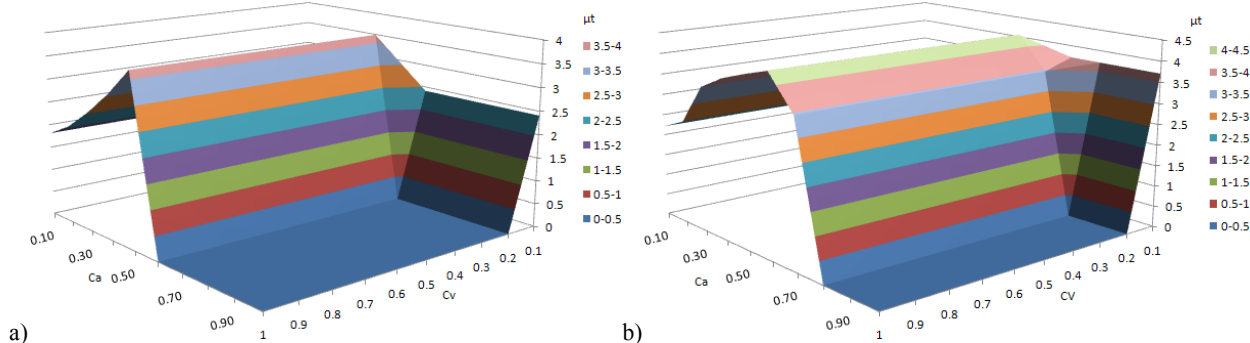


Figure 14. Values of ductility  $\mu_t$  obtained from  $C_a$  and  $C_v$  parameter analysis of target displacement for applied seismic forces as pushover load: a) CSM method, b) ELM method.

Slika 14. Vrednosti duktilnosti  $\mu_t$  dobijenih preko  $C_a$  i  $C_v$  parametarske analize pomeranja tačke za primenjene seizmičke sile kao *pushover* opterećenje: a) CSM metoda, b) ELM metoda

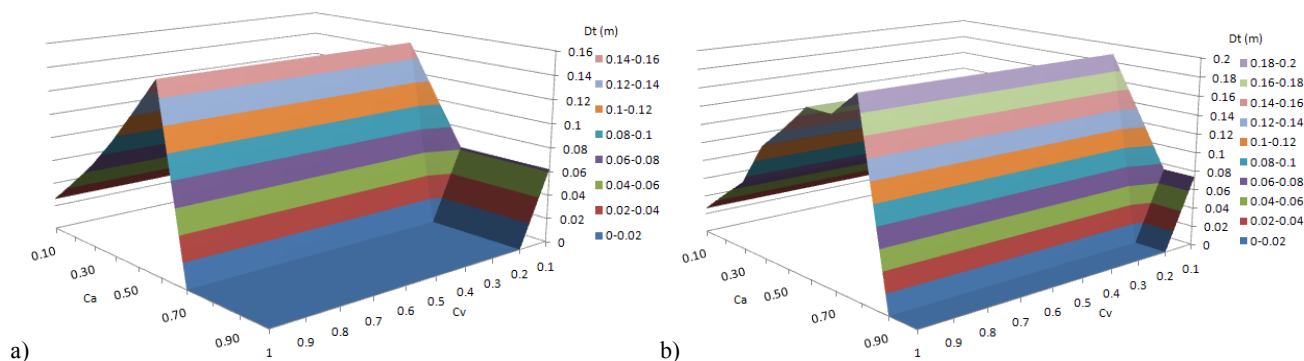


Figure 15. Values of displacement  $D_t$  obtained from  $C_a$  and  $C_v$  parameter analysis of target displacement for inertial seismic forces as pushover load: a) CSM method, b) ELM method.

Slika 15. Vrednosti pomeranja  $D_t$  dobijenih preko  $C_a$  i  $C_v$  parametarske analize pomeranja tačke za primenjene seizmičke sile kao *pushover* opterećenje: a) CSM metoda, b) ELM metoda

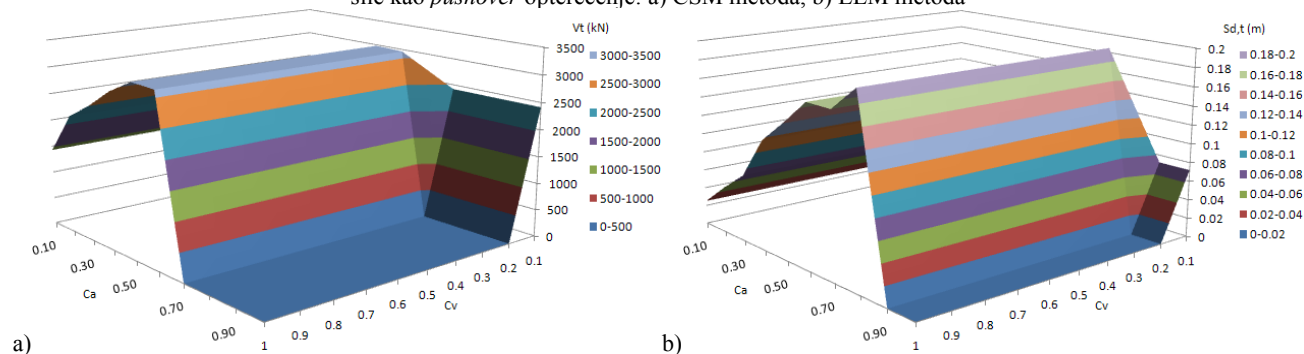


Figure 16. Values of shear force  $V_t$  obtained from  $C_a$  and  $C_v$  parameter analysis of target displacement for inertial seismic forces as pushover load: a) CSM method, b) ELM method.

Slika 16. Vrednosti sila smicanja  $V_t$  dobijenih preko  $C_a$  i  $C_v$  parametarske analize pomeranja tačke za primenjene seizmičke sile kao *pushover* opterećenje: a) CSM metoda, b) ELM metoda

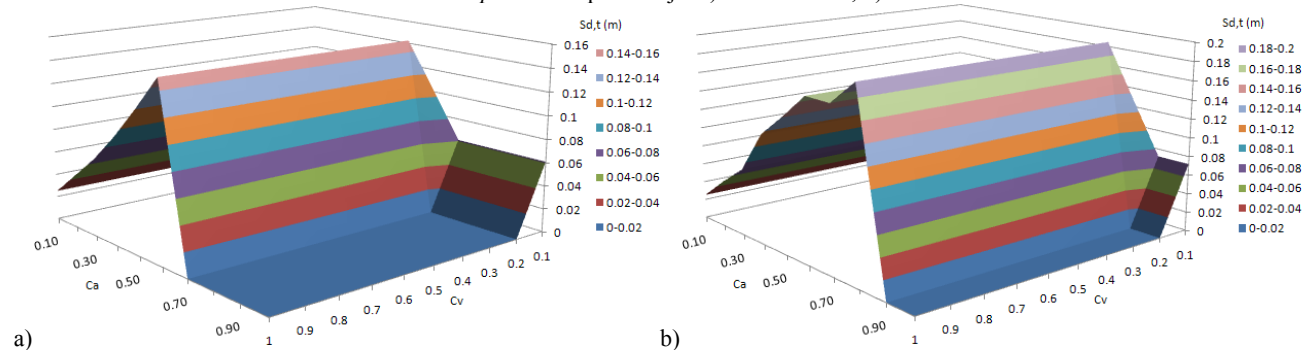


Figure 17. Values of spectral displacement  $S_{d,t}$  obtained from  $C_a$  and  $C_v$  parameter analysis of target displacement for inertial seismic forces as pushover load: a) CSM method, b) ELM method.

Slika 17. Vrednosti spektra pomeranja  $S_{d,t}$  dobijenih preko  $C_a$  i  $C_v$  parametarske analize pomeranja tačke za primenjene seizmičke sile kao *pushover* opterećenje: a) CSM metoda, b) ELM metoda

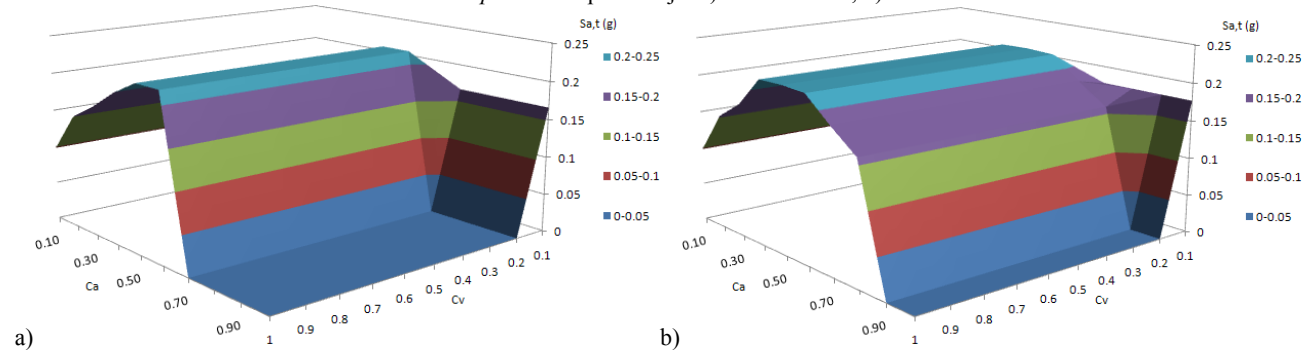


Figure 18. Values of spectral acceleration  $S_{a,t}$  obtained from  $C_a$  and  $C_v$  parameter analysis of target displacement for inertial seismic forces as pushover load: a) CSM method, b) ELM method.

Slika 18. Vrednosti spektra ubrzanja  $S_{a,t}$  dobijenih preko  $C_a$  i  $C_v$  parametarske analize pomeranja tačke za primenjene seizmičke sile kao *pushover* opterećenje: a) CSM metoda, b) ELM metoda

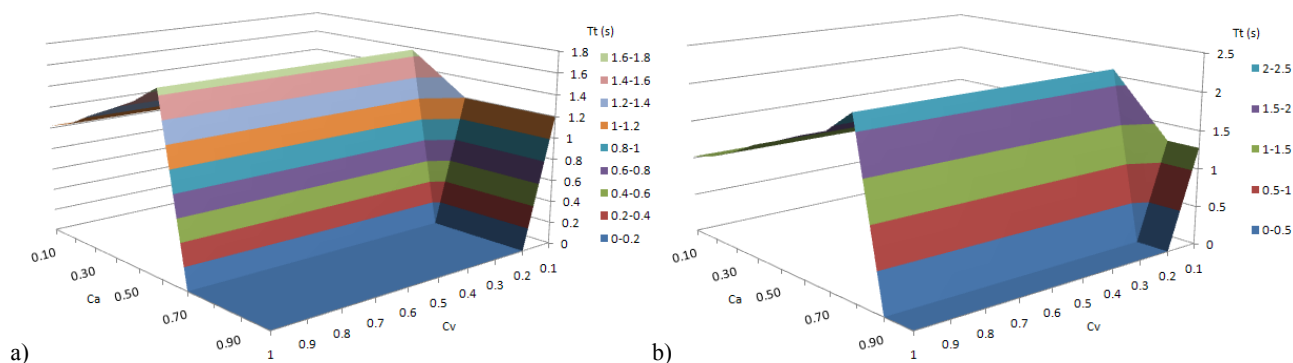


Figure 19. Values of vibration period  $T_t$  obtained from  $C_a$  and  $C_v$  parameter analysis of target displacement for inertial seismic forces as pushover load: a) CSM method, b) ELM method.

Slika 19. Vrednosti perioda vibracija  $T_t$  dobijenih preko  $C_a$  i  $C_v$  parametarske analize pomeranja tačke za primenjene seizmičke sile kao *pushover* opterećenje: a) CSM metoda, b) ELM metoda

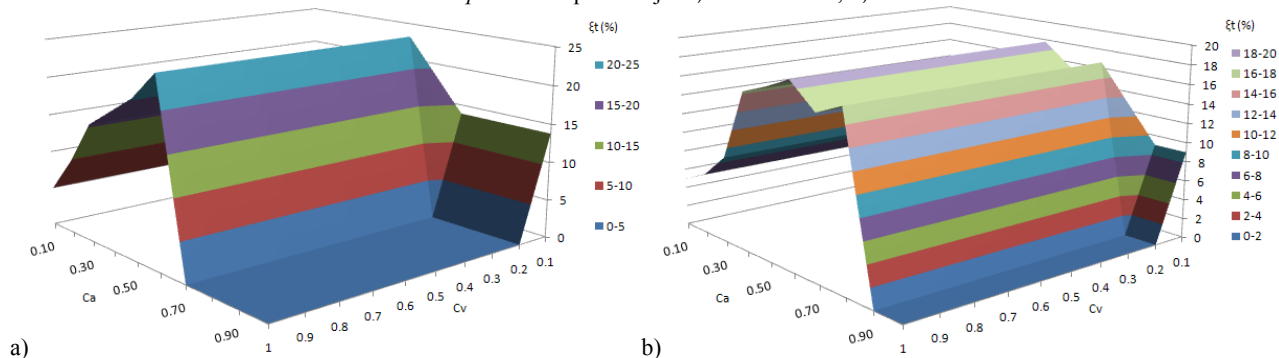


Figure 20. Values of damping  $\xi_t$  obtained from  $C_a$  and  $C_v$  parameter analysis of target displacement for inertial seismic forces as pushover load: a) CSM method, b) ELM method.

Slika 20. Vrednosti prigušenja  $\xi_t$  dobijenih preko  $C_a$  i  $C_v$  parametarske analize pomeranja tačke za primenjene seizmičke sile kao *pushover* opterećenje: a) CSM metoda, b) ELM metoda

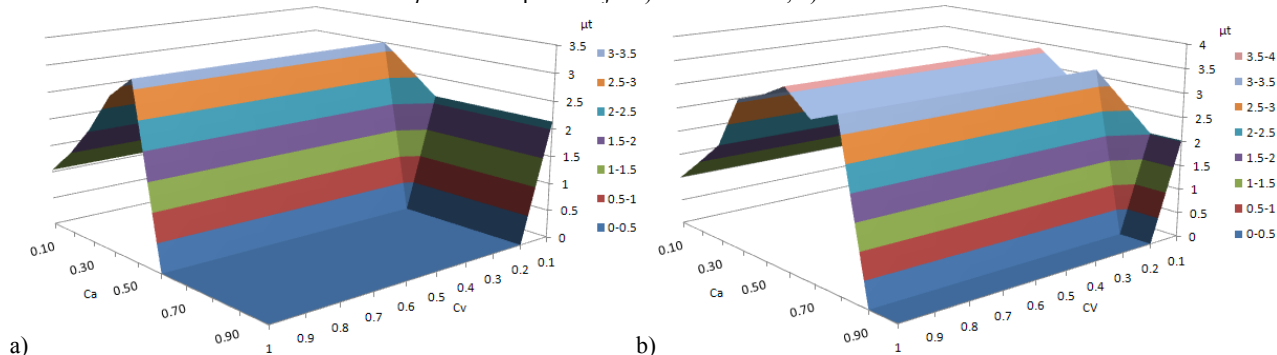


Figure 21. Values of ductility  $\mu_t$  obtained from  $C_a$  and  $C_v$  parameter analysis of target displacement for inertial seismic forces as pushover load: a) CSM method, b) ELM method.

Slika 21. Vrednosti duktilnosti  $\mu_t$  dobijenih preko  $C_a$  i  $C_v$  parametarske analize pomeranja tačke za primenjene seizmičke sile kao *pushover* opterećenje: a) CSM metoda, b) ELM metoda

By analyzing the previous diagrams, it can be concluded that in case of modelling with inertial seismic forces as pushover load, for the purpose of calculating of target displacement levels, values of displacement, total shear force, spectral displacement and acceleration are higher, as compared to other cases. On the other hand, applying ELM method, in comparison to CSM method, resulted in higher values for all considered parameters, except damping. Parameter  $C_a$  and  $C_v$  analysis of target displacement realised the following highest values: displacement  $D_t \approx 0.2$  m, total shear force  $V_t \approx 3500$  kN, spectral displacement  $S_{d,t,max} \approx 0.2$  m, spectral acceleration  $S_{a,t,max} \approx 0.25g$ , vibration period  $T_{t,max} \approx 2.5s$ , damping  $\xi_{t,max} \approx 25\%$  and ductil-

ity  $\mu_{t,max} \approx 5$ . Level of damping, determined using the target displacement analysis, is significantly higher than the initial value. The reason for this is that both viscous and hysteresis damping takes part in this damping. Vibration period of the system for the first mode is  $T_1 = 0.965$  s, which is actually the initial vibration period during target displacement analysis. Since the system is subjected to a gradual development of non-linear strain which leads to stiffness reduction, in this case the vibration period is increased (up to 2.5 times). Ductility, determined by using target displacement analysis, is relatively high, since initiation of system plasticization is realised already during the second step of NSPA.

For standard considerations of a transverse overpass frame, coefficients  $C_a = 0.25$  and  $C_v = 0.4$  are selected, followed by determining of the target displacement level (Table 1). Also, maximal value of system ductility  $\mu_{max}$  is shown for three different procedures of calculating seismic forces. Calculated ductility for target displacement levels is

$\mu_t \approx 3 (> 3)$ , which corresponds to a favourable ductile behaviour, since this ductility is only up to the target displacement level. Total ductility is  $\mu_t \approx 6 (> 6)$ , which confirms the favourable ductile behaviour of the overpass along the transverse direction.

Table 1. Key parameters determined for target displacement levels according to CSM and ELM methods ( $C_a = 0.25$  and  $C_v = 0.4$ ).  
Tabela 1. Parametri određeni za nivoe pomeranja tačke prema CSM i ELM metodama ( $C_a = 0,25$  i  $C_v = 0,4$ )

		$D_t$ (m)	$V_t$ (kN)	$S_{d,t}$ (m)	$S_{a,t}$ (g)	$T_t$ (s)	$\beta_t$ (%)	$\mu_t$	$\mu_{max}$
for applied seismic forces as pushover load	CSM	0.11	2443	0.10	0.17	1.58	19.2	3.07	6.39
	ELM	0.13	2464	0.13	0.17	1.74	19.2	3.82	
for inertial seismic forces as pushover load	CSM	0.09	2878	0.09	0.20	1.37	18.0	2.46	5.833
	ELM	0.12	3150	0.12	0.22	1.47	16.3	3.10	
generation according to the first mode as pushover load	CSM	0.11	2496	0.10	0.17	1.55	19.0	3.05	6.466
	ELM	0.13	2551	0.12	0.18	1.72	19.3	3.83	

Based on previously performed analyses of target displacements for coefficients  $C_a = 0.25$  and  $C_v = 0.4$ , non-linear system strain calculated via developed plastic hinges

as a function of performance state are shown in Figs. 22-24, along with system strain for the level of maximum available displacement.

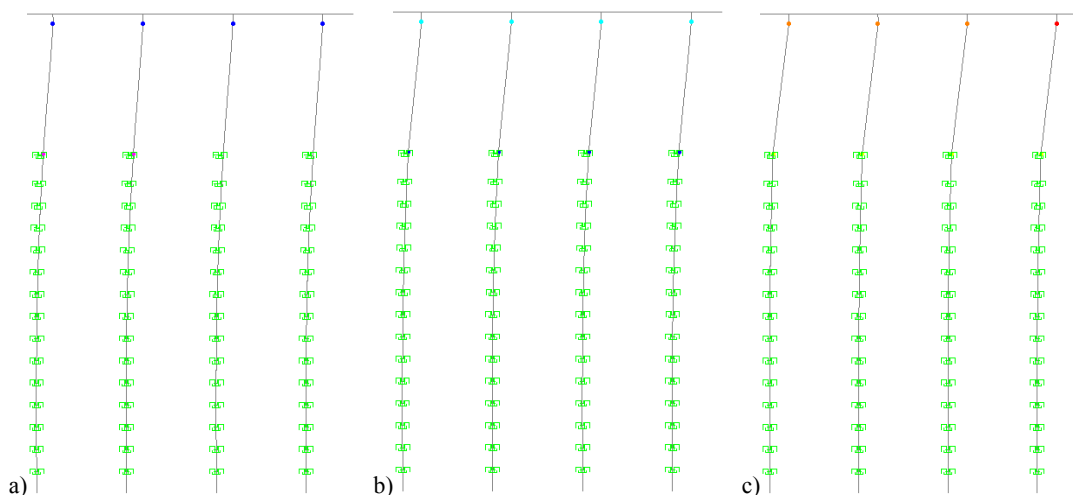


Figure 22. Developed plastic hinges as a function of performance states for applied seismic forces as pushover load: a) target displacement level (CSM method), b) target displacement level (ELM method), c) maximum available displacement level.

Slika 22. Razvoj plastičnih zglobova u funkciji stanja konstrukcije kod primenjenih seizmičkih sila kao *pushover* opterećenje: a) nivo pomeranja tačke (CSM metoda), b) nivo pomeranja tačke (ELM metoda), c) maksimalni raspoloživi nivo pomeranja

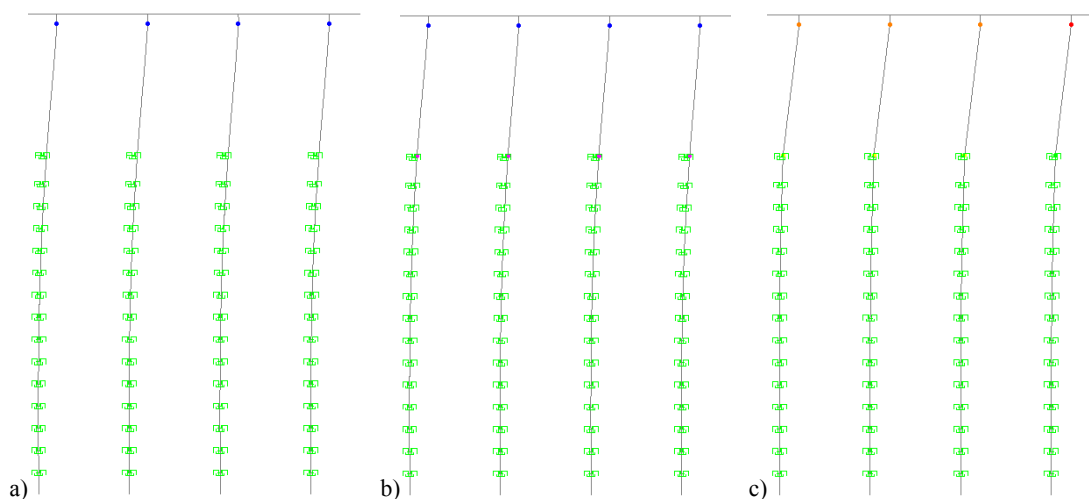


Figure 23. Developed plastic hinges as a function of performance states for inertial seismic forces as pushover load: a) target displacement level (CSM method), b) target displacement level (ELM method), c) maximum available displacement level.

Slika 23. Razvoj plastičnih zglobova u funkciji stanja konstrukcije kod primenjenih seizmičkih sila kao *pushover* opterećenje: a) nivo pomeranja tačke (CSM metoda), b) nivo pomeranja tačke (ELM metoda), c) maksimalni raspoloživi nivo pomeranja

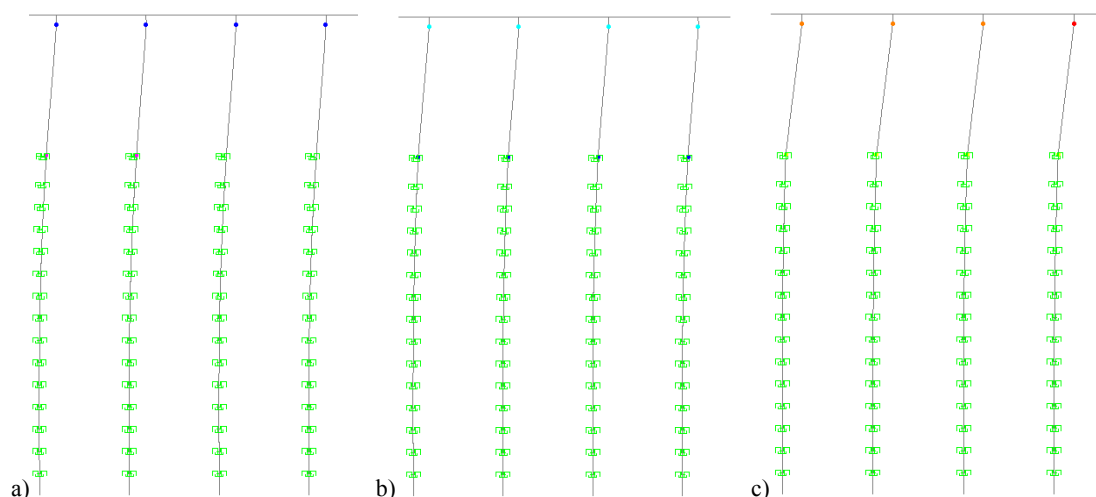


Figure 24. Developed plastic hinges as a function of performance states for inertial seismic forces according to the first mode as pushover load: a) target displacement level (CSM method), b) target displacement level (ELM method), c) maximum available displacement level. Slika 24. Razvoj plastičnih zglobova u funkciji stanja konstrukcije za inercijalne seizmičke sile prema I modu kao *pushover* opterećenje: a) nivo pomeranja tačke (CSM metoda), b) nivo pomeranja tačke (ELM metoda), c) maksimalni raspoloživi nivo pomeranja

It is evident that in these cases, for target displacement levels, the fracture mechanism is formed by plasticization developing at the ends of columns. This fracture mechanism is kept until the maximum available displacement level, with changes in the state of non-linear strain in plastic hinges, while new plastic hinges do not appear. At the level of maximum strain in the bottom part of columns, a performance state that indicates total plasticization occurs. It can be concluded that the fracture mechanism of the overpass occurs due to the appearance of plastic strain in columns, but the levels of damage can be further considered by applying the vulnerability and reliability analysis.

#### VULNERABILITY AND RELIABILITY OF THE OVERPASS IN TRANSVERSE DIRECTION

A deterministic concept of performance analysis of the overpass gives the answers to direct questions regarding the state of the overpass structure. However, probabilistic concept takes into account the level of overpass structure damage as a function of probability of occurrence, i.e. a function of vulnerability probability (*fragility*). Damage levels are considered according to HAZUS, /10/, as: slight, moderate, extensive and complete. These damage levels are defined as a function of system ductility  $\mu$ , in such a way that  $1 < \mu < 2$  corresponds to slight damage,  $2 < \mu < 4$  corresponds to moderate damage,  $4 < \mu < 7$  corresponds to extensive damage and  $\mu > 7$  corresponds to complete damage. A relation between discrete values of spectral acceleration  $S_a$  and ductility  $\mu$  is previously established by using a regression analysis for a linear function. Creating of vulnerability curves is performed in relation to  $S_a$  measure of intensity by applying log-normal distribution, taking into account probability density function and cumulative distribution function. Figure 25a shows discrete probability functions, whereas Fig. 25b shows vulnerability curves for the overpass structure along the transverse direction. Probabilities of initiating  $P > 0$  of corresponding damage levels of the overpass (along the transverse direction) are:  $S_a = 0.03g$  for slight;  $S_a = 0.06g$  for moderate;  $S_a = 0.13g$  for extensive

and  $S_a = 0.16g$  for complete damage. Probabilities of reaching  $P = 1$  of corresponding levels of overpass damage (for transverse direction) are:  $S_a = 0.09g$  for slight;  $S_a = 0.19g$  for moderate;  $S_a = 0.34g$  for extensive and  $S_a > 1g$  for complete damage.

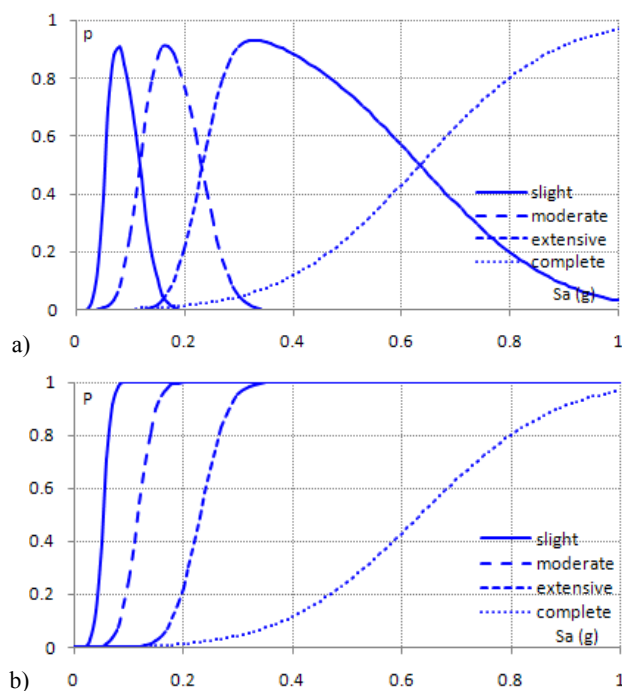


Figure 25. a) discrete probability function, b) vulnerability curves Slika 25. a) diskretna funkcija verovatnoće, b) krive osetljivosti

The system performance assessment, in addition, is performed using reliability state analysis of the overpass. This analysis is based on the previous vulnerability analysis. Figure 26 shows the reliability curves for the overpass structure along the transverse direction. Negative value of coefficient  $R$  indicates the possibility of failure and system unreliability, whereas positive value of this coefficient indicates failure probability close to zero, i.e. significant system reliability. When the value of the coefficient is  $R \approx 6$ , the

system reliability is  $\approx 100\%$ , whereas in case of  $R \approx 0$ , the system failure probability is  $P = 50\%$ . Overpass reliability (along the transverse direction) for  $P > 50\%$  is at  $S_a \leq 0.05g$  for slight damage levels;  $S_a \leq 0.12g$  for moderate damage levels;  $S_a \leq 0.23g$  for extensive damage levels; and  $S_a \leq 0.62g$  for complete damage levels.

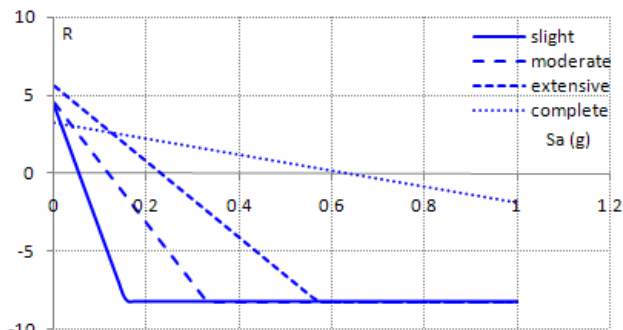


Figure 26. Reliability curves.  
Slika 26. Krive pouzdanosti

## CONCLUSION

Analysis of seismic performances of an overpass along the transverse direction is considered from several aspects: by applying NSPA; target displacement analysis; parameter analysis of target displacement; vulnerability and reliability analyses. Research has determined the maximum value of global drift of 3.5% for columns, whereas for drift values of 2.6%, significant reduction of load bearing capacity. On the other hand, ductility for levels of maximum realized displacement and level of system target displacement are almost larger than 6 and 3, in respect, indicating favourable ductile behaviour. Fracture mechanism development occurs via plasticization of column ends, which also indicates a favourable fracture mechanism for seismic activity conditions. System vulnerability analysis has shown that up to  $S_a = 0.2g$  nearly all levels of damage are initiated, but levels of complete damage ( $P = 1$ ) can be expected only for  $S_a > 1g$ . However, already at values of  $S_a \approx 0.3g$ , extensive damage to the overpass is expected to occur along transverse directions with probability  $P \approx 1$ . Reliability level analysis of the overpass along the transverse direction showed that reliability  $R > 0$  is ensured up to  $S_a < 0.23g$  for levels of extensive damage and lower. Based on that, it can be concluded that the overpass (along the transverse direction) is very vulnerable up to the level of  $S_a \approx 0.3g$ , and that in this case repairs are justified. At higher levels of spectral accelerations, the vulnerability level is noticeably higher, whereas reliability is lower. Based on analyses conceived and performed in this fashion, reliable assessment of damage levels can be conducted, along with plans and analyses of repair measures in case of overpass damage caused by earthquakes.

## ACKNOWLEDGEMENTS

The work reported in this paper is a part of the investigation within the research project supported by the Ministry of Education, Science and Technological Development, Republic of Serbia. This support is gratefully acknowledged (B. Folić and R. Folić).

## REFERENCES

1. AASHTO Guide Specifications for LRFD Seismic Bridge Design, American Association of State Highway and Transportation Officials, USA, 296p, 2012.
2. AASHTO LRFD Bridge Design Specifications, American Association of State Highway and Transportation Officials, USA, 1938p, 2013.
3. ATC 40, Seismic Evaluation and Retrofit of Concrete Buildings, Vol.1, Applied Technology Council, Redwood City, USA, 346p, 1996.
4. Ballard, T., Sedarat, H., *SR5 Lake Washington Ship Canal Bridge Pushover Analysis*, Computers and Structures, Vol.72, Iss.1-3, pp.63-80, 1999.
5. CALTRANS, Seismic Design Criteria, USA, 180p, 2013.
6. Commend, S., *Motorway Exit Bridge3D Pushover Analysis*, GeoMod, 25 years ZSOIL.PC, Lausanne, Switzerland, 2010.
7. Eurocode 8 - Design of Structures for Earthquake Resistance - Part 2: Bridges, European Committee for Standardization, Brussels, Belgium, 150p, 2011.
8. FEMA 440, Improvement of Nonlinear Static Seismic Analysis Procedures, Applied Technology Council (ATC-55 Project), Federal Emergency Management Agency, Washington D. C., USA, 392p, 2005.
9. Folić, R., Projektovanje seizmički otpornih betonskih mostova, Građevinski materijali i konstrukcije, Vol.51, No.2, str.41-65, 2008. (in Serbian)
10. HAZUS, Earthquake Loss Estimation Methodology, National Institute of Building for the Federal Emergency Management Agency, Washington D.C., USA, 1997.
11. Ilić, Đ., Glavni projekat nadvožnjaka na 130 + 003.74 km autoputa E75 Novi Sad-Beograd u sastavu petlje Kovilj, Institut za puteve, Beograd, Srbija, 2006. (in Serbian)
12. Jeffrey, G., Franklin, C., Seismic Design Aids for Nonlinear Pushover Analysis of Reinforced Concrete and Steel Bridges, Taylor & Francis, 376p, 2012.
13. Jones, B., Shenton, H., Effective Width of Concrete Slab Bridges in Delaware, Delaware Center for Transportation, Report, USA, 228p, 2012.
14. Kalkan, E., Kwong, N., *Assessment of Modal Pushover-based Scaling Procedure for Nonlinear Response History Analysis of "Ordinary Standard" Bridges*, ASCE Journal of Bridge Engineering, Vol.17, Iss.2, pp.272-288, 2012.
15. Kornkasem, W., Foutch, D., Long, J., Seismic Behavior of Pile-Supported Bridges, University of Illinois at Urbana-Champaign, Report, USA; 275p, 2001.
16. Mohtashami, E., Shooshtari, A., *Seismic Assessment of Integral Reinforced Concrete Bridges Using Adaptive Multi-Modal Pushover Analysis*, 15 WCEE, Lisbon, Portugal, 2012.
17. Mosher, R., Dawkins, W., Theoretical Manual for Pile Foundations, U.S. Army Corps of Engineers, Report ERDC/ITL TR-00-5, Washington, USA, 2000.
18. PBAB 87, Pravilnik o tehničkim normativima za beton i armirani beton, Beograd, Srbija, 1987. (in Serbian)
19. Pinho, R., Casarotti, C., Antoniou, S., *A Comparison of Single-Run Pushover Analysis Techniques for Seismic Assessment of Bridges*, Earthquake Engineering & Structural Dynamics, Vol.36, Iss.10, pp.1347-1362, 2007.
20. Pravilnik o tehničkim normativima za projektovanje i proračun inženjerskih objekata u seizmički aktivnim područjima, Sl. list SFRJ br. 07, Beograd, Srbija, 1987. (in Serbian)
21. SAP 2000, Integrated Software for Structural Analysis and Design, CSI Berkeley, USA, 2010.
22. Shafiei-Tehrany, R., El Gawady, M., Coffey, W., *Pushover Analysis of I-5 RAVENNA Bridge*, Electronic Journal of Structural Engineering, Vol.11, pp.32-41, 2001.